ISSN 1573-160X, *PHYSICAL OCEANOGRAPHY*, Vol. 31, Iss. 2, pp. 295-316 (2024)
Original Russian Text © The Authors, 2024,
published in *Morskoy Gidrofizicheskiy Zhurnal*, 2024, Vol. 40, Iss. 2, pp. 325–347

Extreme Black Sea Storm in November, 2023

V. A. Dulov, M. V. Yurovskaya ✉, V. V. Fomin, M. V. Shokurov, Yu. Yu. Yurovsky, V. S. Barabanov, A. V. Garmashov

Marine Hydrophysical Institute of RAS, Sevastopol, Russian Federation
✉ *mvkosnik@gmail.com*

Abstract
Purpose. The purpose of the study is to describe comprehensively the extreme storm in the Black Sea in November 2023 in terms of wind and wave field characteristics, based on model calculations, satellite data and field measurements.
Methods and results. The atmospheric fields are calculated using the WRF model, and the wave fields – using the SWAN model. The wind and wave fields, as well as their development during the storm are described in detail. The phenomenon of wave shadowing by the Crimean Peninsula is studied. Using the data available for the storm period, the calculation results are compared to the data from satellite altimeters, the CFOSAT SWIM wave scatterometer and synthetic aperture radars. The data of *in situ* measurements carried out during the storm with the standard equipment of the oceanographic platform in the coastal zone of the Southern Coast of Crimea are presented. The wave characteristics near the oceanographic platform are calculated using the nested grid method.
Conclusions. It was found that during the storm in the Black Sea in November 2023, the maximum wave heights and the maximum wave periods exceeded 9 m and 13 s, respectively. A large amount of satellite data confirmed the calculation results. The results of wave modelling near the oceanographic platform are consistent with in situ measurements. Since the applied configuration of models permitted calculation of the fields of wave physical characteristics with a high degree of reliability, they can be used for an authentic forecast of extreme storms in the Black Sea. The shadowing of waves by the Crimean Peninsula has led to a decrease by a factor of ~ 2 or more in the heights of extreme waves in the coastal waters from the southern tip of the peninsula to Cape Chauda (35.8°E).

Keywords: natural disasters, extreme storm, Black Sea, wind waves, WRF atmospheric model, SWAN wave model, marine *in situ* data, satellite wave altimeters, CFOSAT SWIM wave scatterometer, oceanographic platform

Acknowledgments: The work was carried out within the framework themes of state assignments of FSBSI FRC MHI FNNN-2024-0001, FNNN-2022-0002, FNNN-2024-0012, FNNN-2024-0014, FNNN-2024-0016 and grant No. 169-15-2023-002 of Federal Service for Hydrometeorology and Environmental Monitoring, dated 03.01.2023. The authors are thankful to E.M. Lemeshko, the head of the Black Sea hydrophysical subsatellite polygon of Marine Hydrophysical Institute of RAS for providing the video records of storm waves.

For citation: Dulov, V.A., Yurovskaya, M.V., Fomin, V.V., Shokurov, M.V., Yurovsky, Yu.Yu., Barabanov, V.S. and Garmashov, A.V., 2024. Extreme Black Sea Storm in November, 2023. *Physical Oceanography*, 31(2), pp. 295-316.

Introduction

On 25–27 November 2023, there was a storm with extremely strong wind waves in the Black Sea, causing significant destruction of embankments, piers and coastal structures. In particular, the building of the Institute of Biology of the Southern Seas of the Russian Academy of Sciences was damaged in Sevastopol Bay, which led to

the death of about 500 rare marine animals. Several concrete piers were destroyed in the Sevastopol area, the village of Lyubimovka and the surrounding area of the Chersonesus Lighthouse were flooded. Serious destruction took place on the Southern Coast of Crimea (SCC) and on the Caucasian coast of the Black Sea. The media called this natural disaster the "storm of the century." Such a high-profile incident requires discussion from the viewpoint of oceanology and a detailed description in terms of physical quantity fields.

Information about the evolution of wave characteristic fields at the sea scale follows from wave modelling based on wind speed data from atmospheric models. Modern satellite methods of ocean sounding, as well as contact measurement data, make it possible to verify modelling results and confirm their reliability. A case study of the November "storm of the century" in the Black Sea, combining catastrophic event modelling and available measurement data, has obvious practical significance.

Extreme Black Sea storms were described in a number of works as part of the study of the Black Sea wind-wave regime using the data from wavegauge measurements at weather stations [1, 2], numerical modelling of wave fields [3–7] and estimates of the wave energy potential in the Black Sea [8, 9]. Some examples of model calculations for specific extreme storms are given in [7, 10, 11]. The current level of research into both wind-wave climate and extreme storms involves a combined analysis of the results of numerical modelling, satellite and contact measurements [12, 13]. A comparison of the results of wave modelling in the Black Sea with contact measurements was carried out in [5, 14–16] and with satellite altimeter data in [16–18]. For extreme storms in the listed studies, the maximum values of significant wave heights were 10–12 m. The comparisons of model calculations with satellite and contact data cover large time intervals, as a result, the contribution of extreme storms in this type of research is relatively small. Therefore, confirming the adequacy of modelling the events of extreme storms remains a critical problem.

The present paper gives a case study of the Black Sea catastrophic storm of 25–27 November 2023. Its in-depth development is presented below based on simulations using the WRF atmospheric model and the SWAN wave model. The attention to the wind field is due to the critical importance of its features for the wave field formation. A detailed description of the model configurations with a list of the used parameterizations of physical processes is given to reproduce the results discussed below. The calculations were verified using a large amount of available satellite measurement data. If altimetry estimates of wave heights have previously been repeatedly used in studies of waves in the Black Sea, the SWIM radar data from the CFOSAT satellite is apparently used for the first time to estimate directions and wavelengths in the Black Sea. The paper presents field wave measurement data from the oceanographic platform of the Black Sea hydrophysical subsatellite polygon of Marine Hydrophysical Institute (MHI) of RAS, covering the entire storm period. The purpose of the work is to provide a detailed description of the wave field evolution during the event and to carry out the most accurate verification of the results using satellite and *in situ* data.

Data and models

Regional WRF atmospheric model. The MHI operational atmospheric forecast system based on the WRF model operates in MHI to provide data (heat, moisture and momentum flows on the sea surface) for the Black Sea circulation model in the MHI Marine Forecast Center, as well as for other scientific research in the field of atmospheric interaction and seas in the region. To reproduce such mesoscale phenomena correctly as, for example, breezes, local winds such as boras and local eddies, a spatial resolution of 5–10 km is required because publicly available forecast arrays do not have the necessary detail. The technology of calculating meteorological parameters based on numerical data solving basic equations of thermo- and hydrodynamics for a limited area within the framework of the WRF-ARW mesoscale model is used. The results of the NCEP/NCAR operational global atmospheric forecast in the USA, carried out every 6 hours for 16 days in advance, were used as input data. These data, abbreviated as GFS and publicly available at https://www.nco.ncep.noaa.gov, have a spatial resolution of 0.25°, a 6-hour time resolution and 44 vertical levels. The WRF-ARW model (version 4.5) deployed at the MHI cluster was used. The modelling domain with a horizontal grid step of 9 km included the waters of the Black and Azov seas and the Crimean Peninsula, as well as the waters of the Caspian, Marmara, Aegean and partly Mediterranean seas. The domain grid was 368 × 203 nodes and 45 vertical levels. To parameterize the atmospheric planetary boundary layer, the Mellor-Yamada-Janjic scheme was chosen, the Tiedke scheme – to parameterize cumulus convection, the RRTMG scheme – to calculate radiative transfer in the atmosphere and the Thompson scheme – to calculate phase transitions of water and ice and the transport of hydrometeors in clouds. A four-layer NOAH soil model was used to determine heat and moisture fluxes on the land surface. Documentation for the model with a detailed description of parameterizations is available at https://www2.mmm.ucar.edu/wrf. The fields of meteorological parameters were calculated for the period from 24 November 2023 (00:00) to 28 November 2023 (00:00) (UTC time is given here and below).

SWAN wave model. In this study, the Simulating WAves Nearshore Model Cycle III version 41.45 (SWAN) [19, 20] was used to calculate characteristics of extreme waves. It has already been used in MHI to study extreme storm situations in the Azov-Black Sea basin [3, 6, 21, 22]. The SWAN model belongs to the third-generation spectral models and considers wind input, non-linear quadruplet wave-wave interactions, dissipation of energy due to whitecapping and bottom friction, as well as wave breaking[1] at critical depths. For the wave model input, wind speed U_{10} at a height of 10 m was specified from the WRF atmospheric model. Friction speed at the wave generation source was determined by the aerodynamic formula

[1] SWAN. *Scientific and Technical Documentation. SWAN Cycle III Version 41.45AB.* 2023. [online] Available at: swanmodel.sourceforge.io/online_doc/swantech/swantech.html [Accessed: 10 April 2024].

$u_* = \sqrt{C_d} U_{10}$, where drag coefficient C_d was approximated by a polynomial of the second degree with respect to U_{10} [23]. The process of whitecapping was described by the model in the formulation [24], bottom friction was determined based on the relations from [25]. The angular resolution of the model was 10°. The frequency coordinate used 36 nodes. Minimum frequency was f_0 = 0.033 Hz. Other frequencies were determined using the formula $f_n = 1.1\, f_{n-1}$ ($n \geq 1$). Integration over time was carried out using an implicit difference scheme with a step of 30 minutes in the parallel computing mode on the MHI cluster.

The frequency-angular spectra of waves $S(f, \vartheta)$ were calculated from 24 November (00:00) to 28 November (00:00). The fields of significant wave height $H_S = 4\sqrt{\iint S(f, \vartheta) df d\vartheta}$, the direction of waves ϑ_p at the frequency of spectral peak f_p and the period of the spectral peak waves $T = 2\pi/f_p$ were used for analysis. Below, the H_S, ϑ_p and T characteristics will be called the height, direction and wave period for brevity.

Field measurements were carried out from a stationary oceanographic platform of the Black Sea hydrophysical subsatellite polygon of MHI located approximately 500 m away from the coast, where the sea depth is about 28 m. In Fig. 1, *a*, the platform position is marked by a red asterisk on the satellite optical image from https://www.arcgis.com/apps/View/index.html?appid=504e3ff67457481e839bb941a709350f. The image is also overlaid with ETOPO1 1 Arc-Minute Global Relief Model bathymetry from https://www.ncei.noaa.gov/products/etopo-global-relief-model. Meteorological and wavegauge measurements were carried out in the background mode using a Davis Vantage Pro 2 weather station and a string wave gauge with data transmitted to the shore via a radio channel [14, 26]. Based on successive 20-minute fragments of wave records in the standard way [27], the frequency spectra of waves $S(f)$, the height of significant waves $H_S = 4\sqrt{\int S(f) df}$ and the frequency of spectral peak waves f_p were estimated.

Figure 1, *b* shows a video capture made in the automatic mode on 26 November during a storm at 14:00–14:20. Three vertical structural elements, highlighted in color, were used as an array of "optical wave gauges." The water level on the corresponding vertical lines was converted into vertical displacements of the sea surface at three points using the known exact position of the video camera and its optical parameters. The triangle in the figure shows a virtual plane connecting these points, which gives large-scale wave slopes in two orthogonal directions. Thus, these data are similar to the data of a standard wave buoy[2], and their processing by the triplet analysis method [28] enables us to estimate the frequency-angular spectrum of waves for the video recording time period (a more detailed description of the estimation method is given in [29, 30]).

[2] Earle, M., 1996. *Nondirectional and Directional Wave Data Analysis Procedures.* NDBC Technical Document 96-01. Slidell, USA : Stennis Space Center, 43 p.

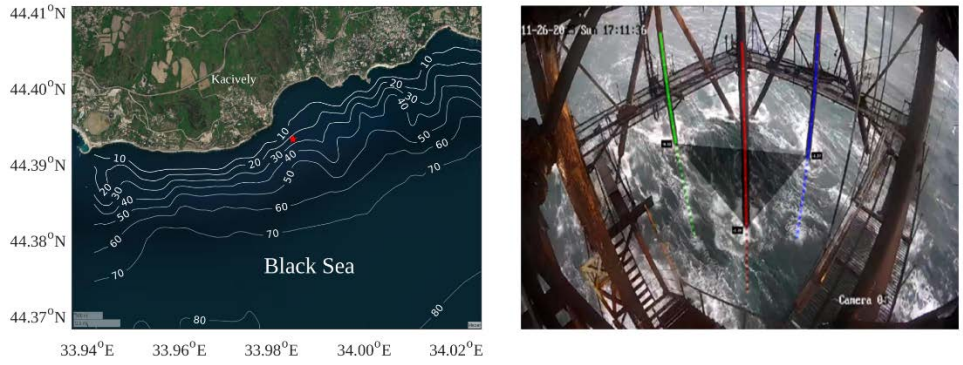

a *b*

F i g. 1. Location of the oceanographic platform (marked with a red asterisk) (*a*) and the platform piles (highlighted in color) as wave gauges (*b*)

Satellite measurements. The work uses the data from altimeters, the CFOSAT SWIM wave scatterometer and synthetic aperture radar (SAR) during the storm. Altimeters are traditionally used to measure wave heights [12]. The altimetry data were taken from the open archives of the Copernicus Marine Environment Monitoring Service (CMEMS) available at https://data.marine.copernicus.eu/product/WAVE_GLO_PHY_SWH_L3_NRT_014_001/description. Capabilities of the SWIM cone-scanning radar [31] installed on the Chinese-French CFOSAT satellite are currently the subject of intensive research [32, 33]. The SWIM instrument is designed to obtain estimates of the spatial spectrum of waves, which, however, turned out to be very noisy [31]. Therefore, only the directions and wavelengths of the spectral peak were used in this study – the CFOSAT SWIM Level-2 data from https://data-cersat.ifremer.fr/projects/iwwoc/. SAR images traditionally used in marine research make it possible to monitor the fields of surface wind speed at a qualitative and quantitative level [34]. Besides, they contain images of dominant wind waves [35]. C-band SAR images are not affected by clouds, which is especially important in extreme weather conditions when the sea is covered by heavy clouds. The three C-band SAR images used were obtained from https://browser.dataspace.copernicus.eu. The information on all satellite data is summarized in Table 1. Altimeter and CFOSAT SWIM radar tracks are shown in Fig. 2.

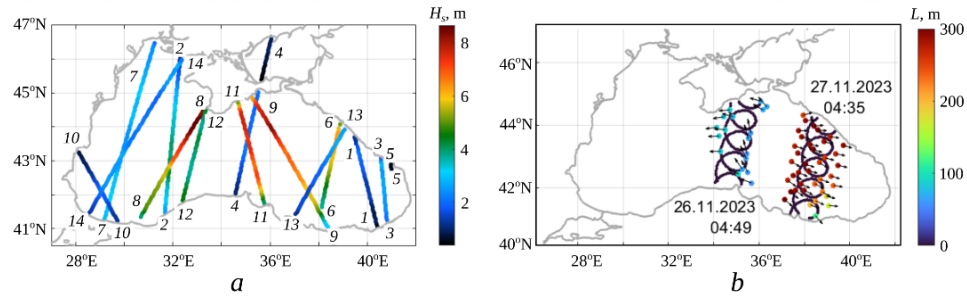

a *b*

F i g. 2. Measurement data: *a* – satellite altimeter tracks indicating wave heights H_S; *b* – tracks of the SWIM sensor (CFOSAT) with indicated direction (arrows) and wavelengths *L* (color)

Table 1

Satellite data

Physical characteristic, sensor	Satellite	Track number	Time of flight
Wave height, altimeter	*SARAL-AltiKa*	*1*	02:41 (26.11)
	CryoSat-2	*2*	09:05 (26.11)
	CryoSat-2	*3*	20:14 (26.11)
Wave direction and wavelength, SWIM, wave height, altimeter	*CFOSAT*	*4*	04:49 (26.11)
	CFOSAT	*5*	15:30 (26.11)
	CFOSAT	*6*	04:35 (27.11)
Wave height, altimeter	*HaiYang*-2*B*	*7*	04:41 (27.11)
	HaiYang-2*C*	*8*	20:23 (26.11)
	JASON-3	*9*	21:46 (26.11)
	JASON-3	*10*	22:08 (27.11)
	Sentinel-3*A*	*11*	19:06 (26.11)
	Sentinel-3*B*	*12*	08:21(27.11)
	Sentinel-6*A*	*13*	12:59 (26.11)
	Sentinel-6*A*	*14*	13:21 (27.11)
Normalized radar cross-section, SAR	*Sentinel*-1*A*	–	04:06 (26.11)
	Sentinel-1*A*	–	15:20 (26.11)
	Sentinel-1*A*	–	03:17 (27.11)

Overall picture of the storm in the Black Sea

Wind field. The weather in the Black Sea region on 25–26 November 2023 was determined by a powerful extratropical cyclone with the center moving from the Balkan Peninsula through the Black Sea to Crimea and further to the north. Analysis of archived fields of sea level pressure, geopotential and the temperature on 25–27 November 2023 gives the following scenario for cyclone formation. The cyclone originated on the southeastern boundary of a deep, meridionally elongated trough in an area of strong horizontal temperature gradient. An intense and fairly compact cyclone is formed to the southeast of the trough, manifesting in the pressure field at sea level. Fig. 3, a shows its trajectory and pressure at sea level at its center (in hPa) according to the calculations using the WRF model. The time intervals between the graph points are 6 hours, the starting point (in the southwest) corresponds to 25 November 2023 (00:00). Cyclones with a similar trajectory are typical for the Black Sea region; traditionally they are called “southern” cyclones. They form over the Mediterranean Sea, move northeast, pass over the western part of the Black Sea and then move north across the territory of Russia. This type of Black Sea cyclone includes the well-known storm of 10–11 November 2007, which led to catastrophic consequences. It had almost the same trajectory and the maximum wind speed reached 30 m/s [36].

Figures 3, *b* – *e* show the wind fields over the Black Sea according to the calculations using the WRF model. Fig. 3, *b* demonstrates a very complex wind field: the hurricane enters the southwestern sector of the Black Sea against the background of a south-southeast storm wind with an area of maximum values above 20 m/s, occupying the central and eastern parts of the sea. In Fig. 3, *c* the hurricane is moving over the Black Sea to the north-northeast while maintaining

a south-southeast wind in the eastern Black Sea. In Fig. 3, *d*, the "eye" of the hurricane reaches the western tip of Crimea; over the Black Sea to the west of 37°E, the wind field acquires a clearly defined cyclonic "centrally symmetric" structure, typical for tropical cyclones. Fig. 3, *e* corresponds to the moment of time after the hurricane makes landfall – the cyclonic wind field covers the Black Sea almost completely. Then, over time, the wind speed decreases as the hurricane moves away from the sea.

In Fig. 3, *f*, model calculations are confirmed by available satellite radar images. Against the light background of the images, corresponding to land backscatter and sea surface scattering at high wind speeds, dark areas of the absence of storm winds are distinguished. At 04:14 on 26 November (left photo), a dark area elongated between 43° and 44°N coincides with the line of change in wind speed direction (occlusion front), emanating from the "eye" of the hurricane and is clearly seen in Fig. 3, *b*. At 15:20 (right photo), a cold front is visible between the stormy and moderate wind zones, shown in the model field for 15:00 in Fig. 3, *d*.

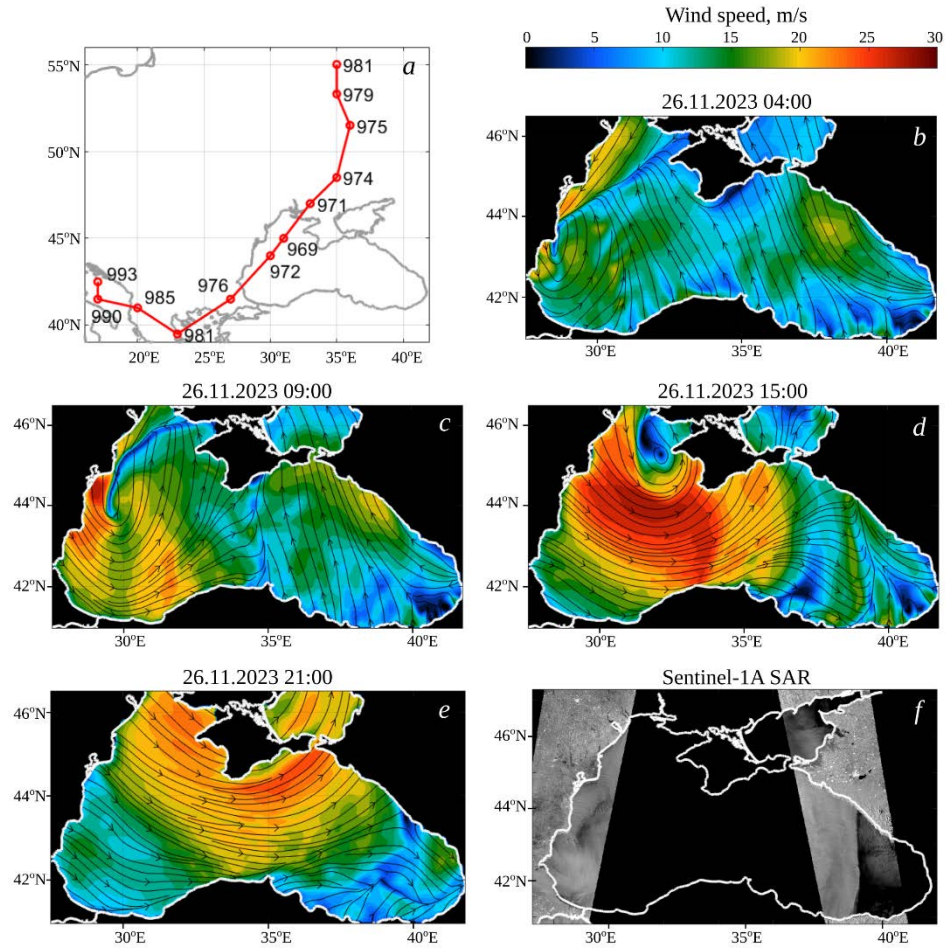

F i g. 3. Atmospheric characteristics: hurricane track and sea level pressure in its center (*a*); streamlines and wind speed on 26 November at 04:00 (*b*), 09:00 (*c*), 15:00 (*d*), 21:00 (*e*). Satellite radar images obtained on 26 November at 04:14 (left) and 15:20 (right) (*f*)

Field of wind waves. Figures 4 and 5 show wave field development on 26 November 2023 according to the calculations using the SWAN model for the entire Black Sea on a grid with a resolution of 4.5 × 4.5 km (246 × 160 nodes). Fig. 4, *a* – *d* shows spatial distributions of wave height (color) and direction (arrows) for four moments in time: 13:00, 16:00, 19:00 and 21:00. Figure 5 shows time dependences of wave height and period at six different points of the sea. The positions of the points are shown in Fig. 4, *e*, their coordinates are in the headings of the tabs in Fig. 5. Point *1* was selected in the central part of the sea, points *2* – *6* – several kilometers seaward of Sevastopol, Kaciveli, the Kerch Strait, Novorossiysk and Sochi, respectively.

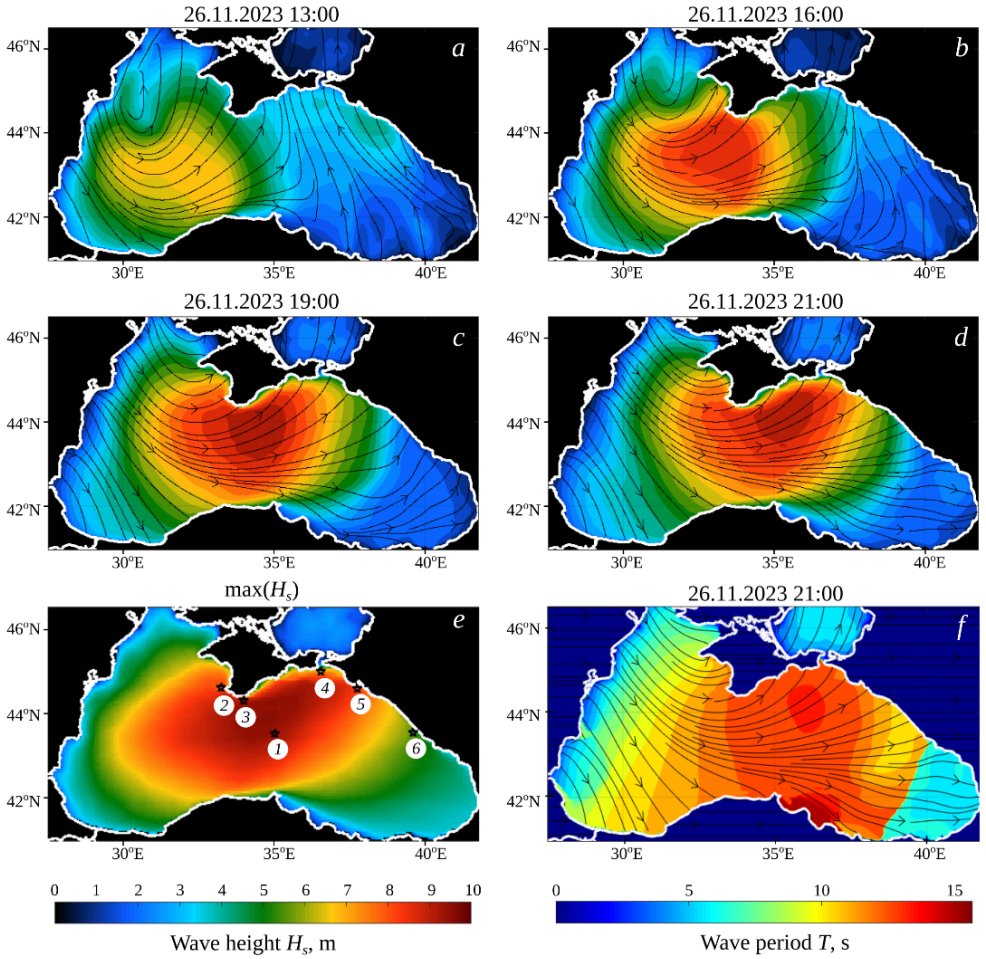

F i g. 4. Field of wind waves: height and direction of waves on 26 November at 13:00 (*a*), 16:00 (*b*), 19:00 (*c*), 21:00 (*d*); distribution of maximum wave heights during the storm period (*e*); periods and directions of waves on 26 November at 21:00 (*f*)

By 10:00, as a result of the hurricane passage through the western part of the sea (Fig. 3, *b*, *c*), an area of storm waves with heights of up to 3 m and periods of up to 8 s, spreading to the east and northeast, is formed. Its boundary has not yet reached the sea center (point *1* in Fig. 5), but near the coast of Crimea (points *2* and *3* in

Fig. 5) the beginning of a monotonous increase in wave height can be seen. At this moment, there are already storm waves generated by a local strong wind near the Caucasian coast of the Black Sea. This area is seen in Fig. 3, *b*, *c*. Accordingly, wave heights are 3–4 m and higher at points *4–6* in Fig. 5.

Further, the storm area boundary moves eastward with increasing height and period of storm waves. By 13:00, wave heights reach 4–5 m (Fig. 4, *a*), a distinct increase in waves begins in the sea center (point *1*) and near Kaciveli (point *3*), and the waves continue to increase near Sevastopol (point *2*). By 16:00, the area of the most intense storm waves covers the entire sea center, wave heights reach 7 m (Fig. 4, *b*). At 19:00, the storm area continues to spread to the east, the wave heights already exceed 9 m (Fig. 4, *c*). Around this time, maximum wave heights are reached in the sea center (point *1*) and Kaciveli (point *3*). The moments of reaching maximum wave heights are highlighted in Fig. 5 by vertical lines. By 21:00, intense storm waves reach the Caucasian coast of the Black Sea (points *4*, *5*). Fig. 4, *d*, *f* shows the fields of wave heights and periods along with wave directions at 21:00. Throughout the entire Black Sea water area, except its western and eastern extremities, a field of developing wind waves is established with propagation directions close to the wind direction shown in Fig. 3, *e*. Wave periods in the sea center reach 11 s or more (Fig. 4, *f*; point *1* in Fig. 5). A storm wave front (Fig. 4, *f*), spreading to the east, is clearly seen in the eastern part of the sea. Around 00:00 on 27 November, the waves reach their maximum heights and maximum periods near Novorossiysk (points *2* and *5* in Fig. 5); near Sochi, storm waves begin to grow (point *6* in Fig. 5). At approximately 04:00 on 27 November, the waves reach their maximum near Sochi (point *6* in Fig. 5). Then, with a gradual decrease in wind speed, the wave height decreases.

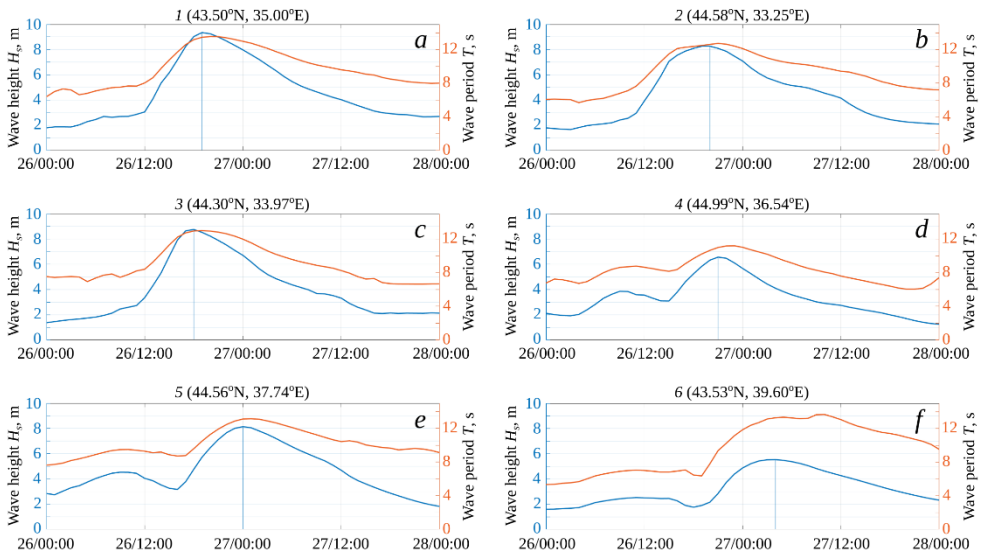

F i g. 5. Dependences of wave heights and periods on time for the points in the sea shown in Fig. 4, *e*: center of the sea (*1*), regions of Sevastopol (*2*), Kaciveli (*3*), Kerch Strait (*4*), Novorossiysk (*5*), Sochi (*6*)

Figure 4, *e* shows the distribution of maximum wave heights over the Black Sea during the storm period. In the sea center, covering almost half of its area, the wave heights exceeded 8 m. The area of waves with heights of 8 m or more covered areas near Sevastopol, Yalta and Novorossiysk, wave heights near Sochi reached 5–6 m. The maximum wave periods exceeded 13 s, and at point *6* in the Sochi region they approached 14 s (Fig. 4, *f*; point *6* in Fig. 5).

Comparison of wave characteristic calculations and satellite data. Figure 6 characterizes the correspondence between model calculations and satellite measurements. Fig. 6, *a*, *c*, *e* shows examples of altimetry data comparison and wave height calculation at the moments of satellite passage. The figures show a certain agreement both in wave height values and in its variability along the track. For example, in the southern parts of all tracks there is a transition from high storm waves in the sea center to moderate height waves on the southern periphery of the storm in accordance with model calculations. In Fig. 6, *a*, both in the model and in the altimetry data, an area of reduced wave height is observed near the coast of Crimea.

In Fig. 6, *b*, *d*, the SWIM radar data from the CFOSAT satellite are superimposed on the fields of wave periods and directions calculated for the moments of satellite passage. The calculation of wave periods T from satellite-measured wavelengths L was carried out using the dispersion relation for linear waves at finite sea depth $T = 2\pi/\sqrt{gk\tanh(kh)}$, where $k = 2\pi/L$; g is gravity; h is sea depth at the point under consideration [37]. In Fig. 6, *b*, *d*, the wave periods calculated from satellite measurements are shown in the form of circles, the color of which corresponds to the color scale, and the measured wave directions are shown by arrows. The time of the first satellite scene (Fig. 6, *b*) corresponds to the pre-storm state of the sea – propagation of waves generated by the wind field that existed there before the storm (see Fig. 3, *b*). The time of the second flight of the satellite corresponds to the active phase of the storm (Fig. 6, *d*), but the wind speed in the area of the southern part of the track at this moment had already dropped to 15 m/s and lower. For the wave periods calculated by the model (13–14 s, see Fig. 6, *d*), the inverse wave age $\alpha = 2\pi U_{10}/(gT)$ does not exceed 0.74, which is lower than the value of 0.83, characterizing the fully developed waves with the Pierson–Moskowitz spectrum [38]. Thus, the waves in the southern part of the track are also swell.

Figure 6, *b* shows correspondence of wave periods with some discrepancy between the calculated and measured wave directions. It is understandable in a situation of mixed waves, when there are simultaneously developing waves from an incipient storm in the eastern part of the sea and a swell coming from the west. Figure 6, *d* demonstrates reasonable agreement between the measurement and simulation results for both the period and the direction of the waves. However, in the southern part of the track, the model calculation overestimates the swell period compared to the measured one. Figure 6, *f* shows a fragment of a satellite SAR image for a point in the eastern part of the sea with coordinates 41.1°E and 42.4°N (27 November 2023, 03:17), where the dominant waves are clearly observed. A 1 km long segment is superimposed on the image. The segment length fits

4 wavelengths, which corresponds to the wavelengths of 250 m and thus to a wave period of 12.7 s. This estimate is consistent with the CFOSAT SWIM measurements, although it is lower than the value obtained from the model (T = 13.95 s). For the considered point, the wind speed according to the WRF model was U_{10} = 9.6 m/s, which gives the inverse wave age α = 0.24, i.e., the waves are definitely a swell. This satellite image confirms the overestimation of the swell wave period by the model calculation.

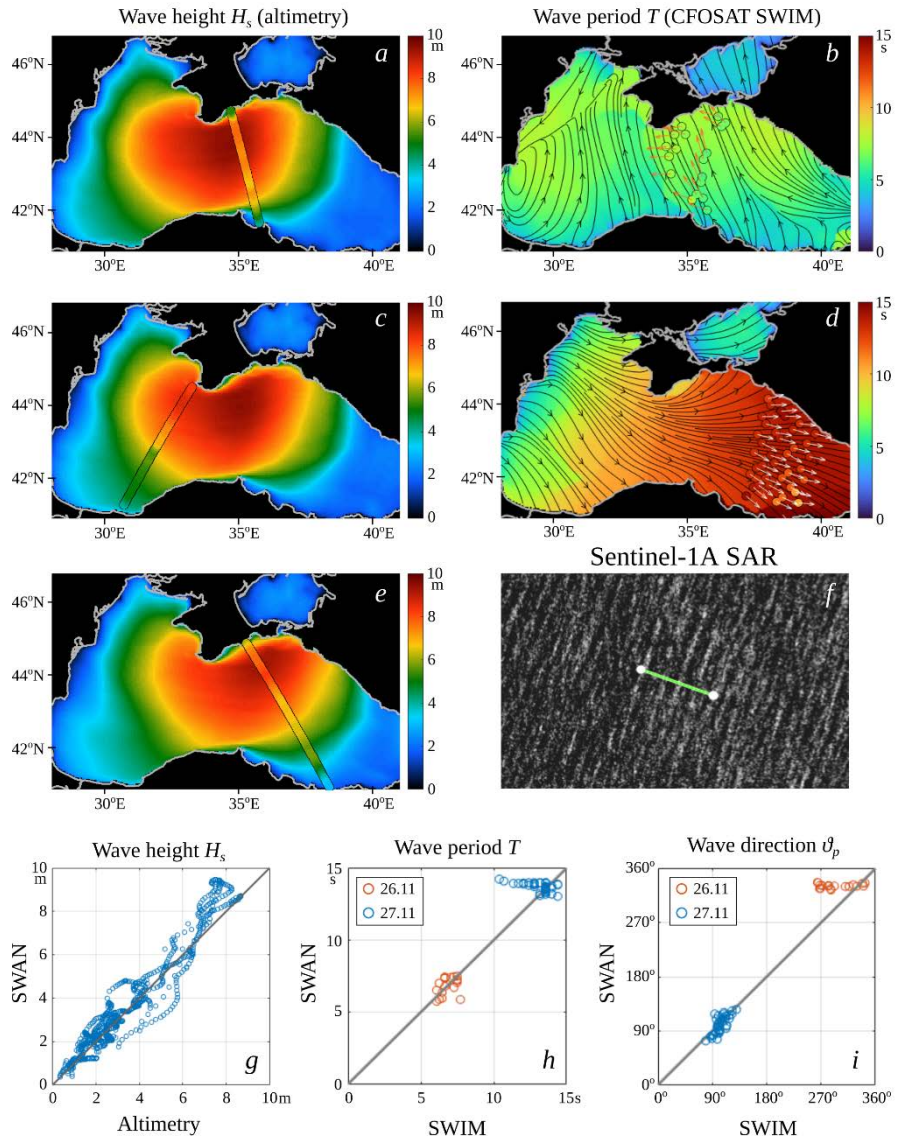

F i g. 6. Comparison of model calculations and satellite data: simulated wave height fields with the superimposed altimeter data from 26 November at 19:06 (*a*), 20:23 (*c*), 21:46 (*e*); simulated fields of wave periods and directions with the superimposed SWIM data from 26 November at 04:49 (*b*) and 27 November at 04:35 (*d*); fragment of SAR image with the superimposed line of 1 km long (*f*). Comparison of simulations and satellite data in terms of wave heights (*g*), periods (*h*) and directions (*i*)

Physical mechanisms of swell dissipation and evolution are not completely understood nowadays [39–41] and parameterizations of swell evolution mechanisms in wave models continue to be improved [42–45]. However, in the SWAN model, the methods for calculating swell and wind waves do not differ [41]. This is probably responsible for the discrepancies in the direction of the swell waves in the first satellite pass and the obvious overestimation by the model of the periods of swell waves in the southern part of the track during the second flight.

Figure 6, $g - i$ summarizes the considerations of this subsection. Figure 6, g shows a comparison with calculations for all altimeter tracks data shown in Fig. 2 and Table 1. Figure 6, *h*, *i*, presents the comparison for all CFOSAT SWIM data by periods and wave directions, respectively, with points for the first and second satellite shown in red and blue. Table 2 shows data correlation coefficients, bias and root-mean-square error calculated from the point clouds in Fig. 6, $g - i$. Note that the error in measuring wave heights with an altimeter for the open ocean is 16 cm [46], but in coastal areas it can increase up to 1.6 m [47]. Recent work [46] validated CFOSAT SWIM data on an extensive array of field measurements, resulting in standard errors (RMSE) for wavelengths and directions over 38 m and 9.1 degrees. At the same time, the residuals for individual measurements can be over 70 m and 20 degrees when observing waves with a length of 225 m (Fig. 5 in [46]). As follows from the dispersion relation for linear waves in deep water, errors in the wavelength δL are related to errors in the wave period by the relation $\delta T = \pi \delta L/(gT)$. That is, an error of 38 m for wave periods of 10–3 s corresponds to errors in period estimation $\delta T \approx 1.2 - 0.9$ s. Thus, we can conclude that our comparison of model calculations with individual satellite measurements shows very reasonable agreement. For the purposes of the present study, it is important that there is a correspondence between the heights and periods of the highest developing waves (H_s = 4–9 m) and the directions of waves in the active phase of the storm.

T a b l e 2

Degree of consistency between the satellite and calculated data

Characteristics of waves	Bias	RMS	Correlation coefficient
Height	0.21 m	0.66 m	0.97
Period	0.48 s	1.4 s	0.92
Direction	9 degrees	26 degrees	0.98

Storm off the Southern Coast of Crimea

The phenomenon of wave shadowing by the Crimean Peninsula. *The* above model calculations highlight an area of decreased wave height in the water area adjacent to the coast from the southern tip of Crimea to Cape Meganom (35.08°E) and further from the Feodosiya Gulf to Cape Chauda (35.8°E) (Fig. 4, $c - e$). In this area, the wave height does not exceed 4–5 m, while more seaward it reaches 8–9 m. The altimetry data confirm the presence of this area (Fig. 6, *a*). According to

the contact measurements from an oceanographic platform located in the western part of the area, the wave height did not exceed 4 m.

The presence of the area is associated with the shadowing of developing wind waves coming from the west by the Crimean Peninsula. The wave field formation in this area involves waves coming from the southwest, as well as young waves generated by local wind, and, possibly, the effects of nonlinear processes and refraction of waves coming from the west and reaching the south of Crimea. However, the shadowing effect in this case plays a major role, since the calculated wave spectra do not contain energetically significant (i.e., significantly affecting the H_S value) wave harmonics propagating to the east.

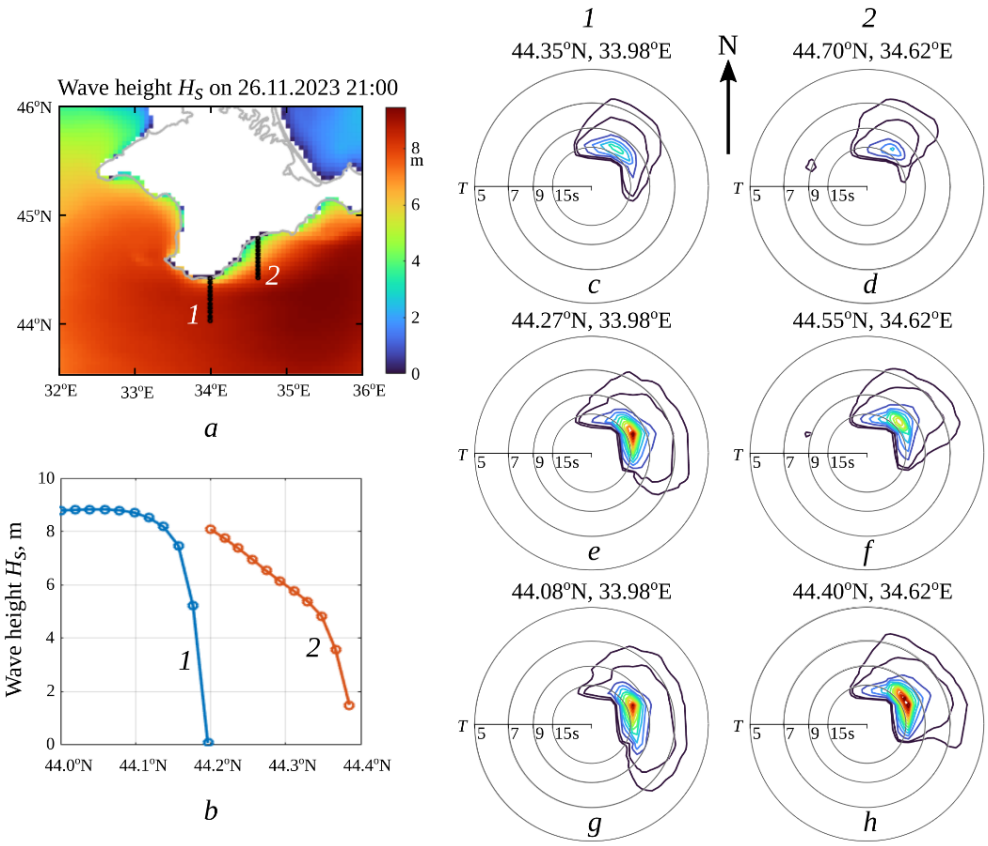

F i g. 7. Shadowing of waves by the Crimean Peninsula: a – transects *1* and *2* superimposed on the simulated field of wave heights; *b* – wave height along transects *1* and *2*; frequency-angular spectra of waves along transects *1* (*c, e, g*) and *2* (*d, f, h*), where the circles (from larger radius to smaller one) correspond to wave periods 5, 7, 9, 15 s

In Fig. 7, this phenomenon is illustrated by latitudinal sections of the wave field, covering spatial regions of the shadowing absence and presence (Fig. 7, *a*, section *1* corresponds to the oceanographic platform longitude). Figure 7, *b* shows variation of wave heights along latitude. Figure 7, *c* – *h* shows changes in the calculated frequency-angular spectra along the transect. In these figures, presented in polar coordinates,

the frequency is plotted along the radius, the geographic azimuth is measured from the direction to the north (in the figure – vertically upward) and shows where the wave harmonic propagates. Spectral density is indicated in arbitrary units.

Domains of the transects are approached by waves developed from the western extremity of the sea, which have a relatively wide angular spectrum. The Crimean Peninsula obscures some of the wave propagation directions, which leads to the vanishing of the corresponding wave harmonics from the spectrum. In the southern part of the transects (Fig. 7, *e*, *g*), the spectra include waves propagating both to the northeast and southeast. In the northern part of the transects (Fig. 7, *c*, *d*), the waves propagating to the southeast are absent due to shadowing. Figure 7, *e*, *f* shows the transition between these states. As a result of "cutting off" the southeastern direction waves from the spectrum, the total wave energy decreases significantly and the wave height decreases from 9 m to ~ 4 m (Fig. 7, *a*, *b*).

Thanks to the shadowing, the damage caused by the storm in the central and eastern parts of the SCC turned out to be significantly lower than it would have been in the absence of this effect.

Wave modelling near the oceanographic platform. The wave measurements taken not far enough from the coast, for example, at Cape Chersonesus or at the oceanographic platform in Kaciveli, strictly speaking, cannot be compared with model calculations on a large grid. Comparison requires calculations on a sufficiently fine grid and the model must adequately take into account the influence of shallow water effects on wave evolution. In [14], a comparison of wave characteristics calculated using the WAM Cycle 4 wave model [48] on a coarse grid with measurements from an oceanographic platform was carried out. Only waves coming from the open sea were considered and as a result a good correspondence was obtained. In this study, in contrast to [14], extreme waves with wavelengths reaching 200 m or more in deep water and significantly exceeding the sea depth of 28 m are considered. In this case, it is fundamentally important to consider the influence of bathymetry details on wave characteristics.

To simulate storm waves in the area of the MHI oceanographic platform on 24–28 November 2023, as before, the SWAN Cycle III model (version 41.45) [1] was used, but to increase the spatial resolution, a four-step nested grid method was applied. At the first step, wave fields were simulated for the entire Black Sea on a grid with a resolution of 4.5 × 4.5 km (246 × 160 nodes). At the second step, waves for the water area including the South Coast on a grid of 0.8 × 1.13 km (234 × 122 knots) were calculated. At the third step, waves were modeled in the coastal zone of the SCC from the village of Ponizovka to Simeiz with a resolution of 200 × 200 m (171 × 198 knots). At the fourth step, with a resolution of 15 × 20 m (118 × 91 knots), the wave fields in the coastal waters of Kaciveli, including the oceanographic platform, were modeled. During calculations at the second, third and fourth steps, the wave parameters at the liquid boundaries of computational domains were determined by interpolating model data from the previous steps. As before, surface wind fields from the WRF mesoscale atmospheric model were used as forcing.

The SWAN model operates in the approximation of geometric optics: the dimensions of inhomogeneities in the medium should significantly exceed the wavelengths. Strictly speaking, the calculation at the fourth modelling step is not completely correct, since the grid step turns out to be smaller than the wavelength. However, the coastline and bottom topography in the water area surrounding the platform experience significant changes at scales of 30–50 m. The fourth calculation step was carried out to consider this variability to some extent in the model. At the same time, the use of a four-step approach ensures the solution continuity when approaching the platform from the open sea.

Field measurement and modelling results. Fig. 8 shows measurement data from the oceanographic platform in comparison with the calculation. Fig. 8, a shows wind speed and direction; Fig. 8, *b* – wave height and period; Fig. 8, *c*, *e* – instantaneous frequency spectrum according to the measurements of the string wave recorder and calculations, respectively; Fig. 8, *d*, *f* – frequency-angular spectra according to the measurements of the "optical" wave recorder and calculations, respectively. The frequency-angular spectra are presented in polar coordinates, where the azimuth the waves come from is indicated.

As follows from these data, on 26 November, from 06:00 to 16:00, the wind direction changes to ~ 255 degrees with a simultaneous increase in its speed (Fig. 8, *a*). In the time period 16:00–18:00, the wind speed is close to the maximum value of 28 m/s and on 27 November from 18:00 to ~ 02:00 it drops to 13 m/s with a constant wind direction. These wind characteristics persist on 27 November until 14:00, after which the wind speed gradually decreases. Fig. 8, a shows the correspondence of the calculated wind speed and its direction to the measured values.

The wave height on 26 November (Fig. 8, *b*) in the time interval 06:00–15:00 increases to 3–4 m and then remains approximately at this level until 19:00. In the time interval 19:00–24:00, the wave height decreases to 1 m. Fig. 8, *b* shows that the model qualitatively correctly describes the temporal variability of wave height and period, although it overestimates these characteristics.

Figure 8, *c* shows changes in the spectral shape of the wave over time, in particular, the evolution of spectral peak frequency. As follows from the figure, the strongest transformation of the spectrum occurred from 10:00 to 14:00. Then, until 22:00, the period of the spectral peak waves was 11.7–12.8 s, corresponding to wavelengths of 167–187 m when recalculated using the dispersion relation for surface waves [37] at a final sea depth of 28 m at the platform location. If we assume that the wave frequency remained the same when approaching the shore, then in deep water these waves had a length of 214–256 m. Comparison of Fig. 7, *c*, *e* demonstrates the correspondence of waves frequency spectra and their temporal variability.

The frequency-angular spectrum assessment (Fig. 8, *d*) shows that the main system waves come from the west (240 degrees), from a direction close to the wind direction indicated by the arrow. At the same time, a system of lower intensity swell waves, which come from the east (~ 90 degrees), is observed. They were generated by the wind field that existed in the central and eastern parts of the sea at the time of the cyclone arrival (Fig. 3, *b* and its discussion) and generated a wave system that

was observed by CFOSAT during its first flight (Fig. 6, *d*). Fig. 8, *d*, *f* shows the agreement of the spatial spectra: the calculation conveys the frequency and direction of the dominant wave system well. The system of swell waves coming from the east, although with some distortions, is also reproduced by the model.

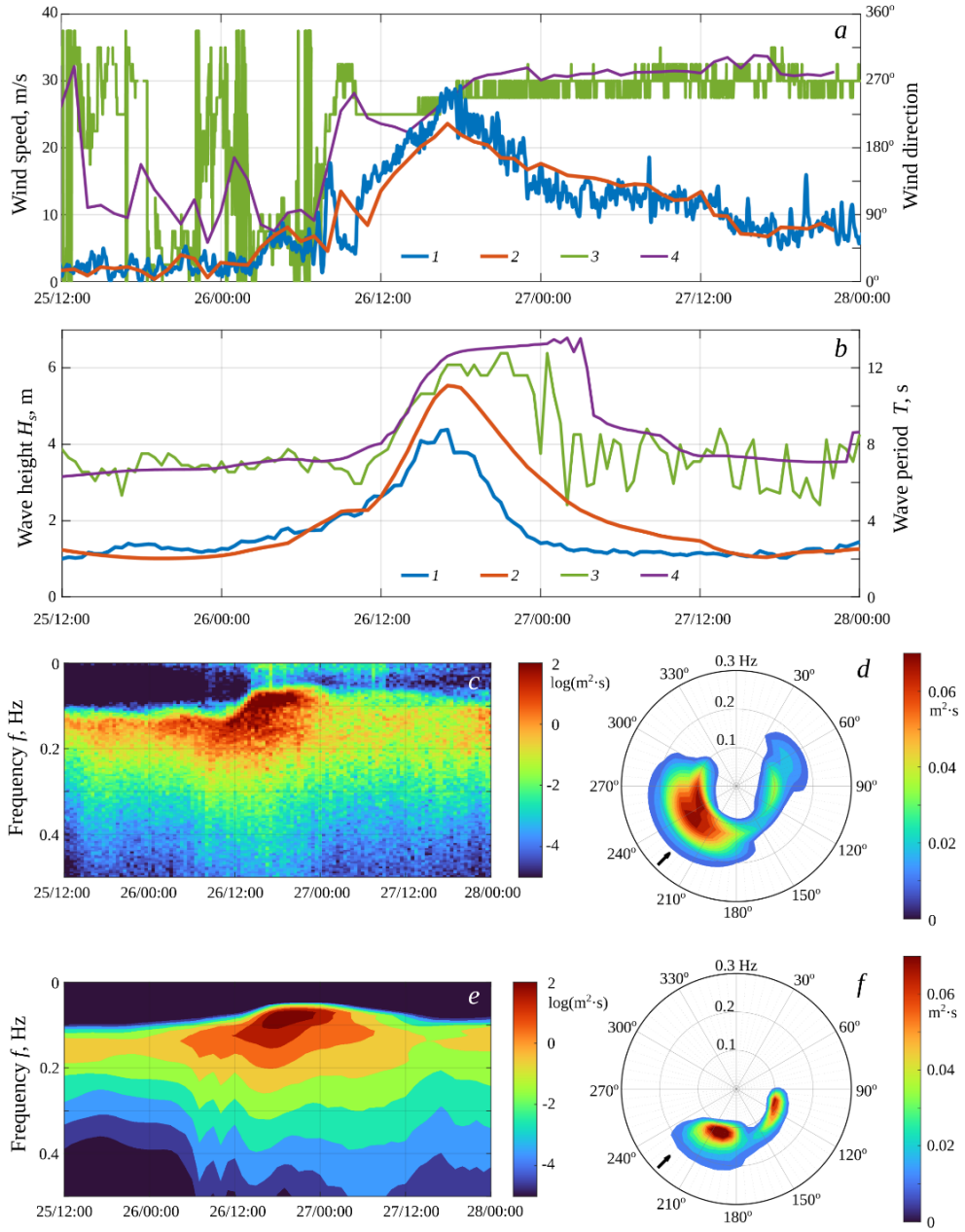

F i g. 8. Shadowing of waves by the Crimean Peninsula: a – transects *1* and *2* superimposed on the simulated field of wave heights; *b* – wave height along transects *1* and *2*; frequency-angular spectra of waves along transects *1* (*c*, *e*, *g*) and *2* (*d*, *f*, *h*), where the circles (from larger radius to smaller one) correspond to wave periods 5, 7, 9, 15 s

Proper operation of the string wave gauge can be confirmed by the presence in its signal of fluctuations of infragravitational frequencies ranging from 0.02 Hz and below (Fig. 8, *c*). These fluctuations are most intense during the period of an "active storm" with the highest wave heights (from 14:00 on 26 November to 09:00 on 27 November) in accordance with generally accepted ideas [49, 50]. The recorded infragravity response of the sea to the storm can be the subject of a special study [51].

Correspondence of the model calculations to the *in situ* measurements from the oceanographic platform can be considered as another confirmation of the model calculation correctness when describing an extreme storm in the Black Sea.

Conclusion

A case study of the November 2023 extreme storm in the Black Sea provided a detailed picture of the storm evolution in terms of physical wave characteristic fields—significant wave heights, directions, and spectral peak wave periods. The atmospheric fields were calculated using the WRF model and the wave fields were calculated using the SWAN model. To verify the modelling results, available data from satellite altimeters, the CFOSAT SWIM wave scatterometer and synthetic aperture radars were used, and SWIM data were used to analyze the Black Sea storm, apparently, for the first time. The data from *in situ* measurements carried out during the storm by standard equipment from the oceanographic platform of the Black Sea hydrophysical subsatellite polygon of Marine Hydrophysical Institute of RAS provided detailed information about the storm at the point of the Crimea coastal zone, where the platform is located. A four-step nested grid method was used to calculate waves near the oceanographic platform using the SWAN model. Thus, a comprehensive study of a specific catastrophic event with extreme wave characteristics was carried out.

A joint analysis of the results obtained prompts the following statements:

– the results of model calculations are confirmed by a large amount of satellite data. The calculation of wave characteristics near the oceanographic platform is consistent with the *in situ* measurements from the platform;

– during the November 2023 storm in the Black Sea, the maximum wave heights and maximum wave periods exceeded 9 m and 13 s, respectively;

– since the used model configurations permitted to obtain the fields of physical characteristics of waves with a high degree of reliability without involving additional sources of information, they can be used for reliable forecasting of extreme storms in the Black Sea;

– shadowing of waves by the Crimean Peninsula led to a decrease in the height of extreme waves by two or more times in the extended coastal waters from the southern tip of the peninsula to Cape Chauda, significantly reducing the dangers and risks associated with the extreme storms there.

REFERENCES

1. Repetin, L.N., Belokopytov, V.N. and Lipchenko M.M., 2003. Winds and Wave Perturbations in the Southwest Crimean Coast. In: MHI, 2003. *Ecological Safety of Coastal and Shelf Zones and*

Comprehensive Use of Shelf Resources. Sevastopol: ECOSI-Gidrofizika. Iss. 9, pp. 13-28 (in Russian).

2. Goryachkin, Yu.N. and Repetin, L.N., 2009. Storm Wind and Wave Regime near the Black Sea Coast of Crimea. In: MHI, 2009. *Ecological Safety of Coastal and Shelf Zones and Comprehensive Use of Shelf Resources*. Sevastopol: ECOSI-Gidrofizika. Iss. 19, pp. 56-69 (in Russian).

3. Divinsky, B.V., Fomin, V.V., Kosyan, R.D. and Ratner, Y.D., 2020. Extreme Wind Waves in the Black Sea. *Oceanologia*, 62(1), pp. 23-30. https://doi.org/10.1016/j.oceano.2019.06.003

4. Divinsky, B.V. and Kosyan, R.D., 2018. Wave Climate of the Coastal Zone of the Crimean Peninsula. *Physical Oceanography*, 25(2), pp. 93-101. https://doi.org/10.22449/1573-160X-2018-2-93-101

5. Akpinar, A. and Bingölbali, B., 2016. Long-Term Variations of Wind and Wave Conditions in the Coastal Regions of the Black Sea. *Natural Hazards*, 84(1), pp. 69-92. https://doi.org/10.1007/s11069-016-2407-9

6. Polonsky, A.B., Fomin, V.V. and Garmashov, A.V., 2011. Characteristics of Wind Waves of the Black Sea. *Reports of the National Academy of Sciences of Ukraine*, (8), pp. 108-112 (in Russian).

7. Efimov, V.V. and Komarovskaya, O.I., 2009. [*Atlas of Extreme Wind Waves of the Black Sea*]. Sevastopol: ECOSI-Gidrofizika, 59 p. (in Russian).

8. Divinsky, B.V. and Kuklev, S.B., 2022. Climate Variations of Certain Wave Parameters at the Inlet of Novorossiysk Bay. *Oceanology*, 62(2), pp. 155-161. https://doi.org/10.1134/S0001437022020035

9. Rusu, L., 2015. Assessment of the Wave Energy in the Black Sea Based on a 15-Year Hindcast with Data Assimilation. *Energies*, 8(9), pp. 10370-10388. https://doi.org/10.3390/en80910370

10. Ivanov, V.A., Dulov, V.A., Kuznetsov, S.Yu., Dotsenko, S.F., Shokurov, M.V., Saprykina, Y.V., Malinovsky, V.V. and Polnikov, V.G., 2012. Risk Assessment of Encountering Killer Waves in the Black Sea. *Geography, Environment, Sustainability*, 5(1), pp. 84-111. https://doi.org/10.24057/2071-9388-2012-5-1-84-111

11. Ivanov, V.A., Shokurov, M.V., Dulov, V.A., Kudryavtsev, V.N. and Soukissian, T., 2013. Atmospheric Modeling for Advance Warning of Weather Disasters in the Black Sea Region. *Geography, Environment, Sustainability*, 6(4), pp. 31-47. https://doi.org/10.24057/2071-9388-2013-6-4-31-47

12. Ardhuin, F., Stopa, J.E., Chapron, B., Collard, F., Husson, R., Jensen, R.E., Johannessen, J., Mouche, A., Passaro, M., [et al.], 2019. Observing Sea States. *Frontiers in Marine Science*, 6, 124. https://doi.org/10.3389/fmars.2019.00124

13. Rusu, E., 2016. Reliability and Applications of the Numerical Wave Predictions in the Black Sea. *Frontiers in Marine Science*, 3, 95. https://doi.org/10.3389/fmars.2016.00095

14. Shokurov, M.V., Dulov, V.A., Skiba, E.V. and Smolov, V.E., 2016. Wind Waves in the Coastal Zone of the Southern Crimea: Assessment of Simulation Quality Based on in Situ Measurements. *Oceanology*, 56(2), pp. 214-225. https://doi.org/10.1134/S0001437016020181

15. Divinsky, B.V. and Kosyan, R.D., 2017. Spatiotemporal Variability of the Black Sea Wave Climate in the Last 37 Years. *Continental Shelf Research*, 136, pp. 1-19. https://doi.org/10.1016/j.csr.2017.01.008

16. Myslenkov, S. and Chernyshova, A., 2016. Comparing Wave Heights Simulated in the Black sea by the SWAN Model with Satellite Data and Direct Wave Measurements. *Russian Journal of Earth Sciences*, 16(5), pp. 1-12. https://doi.org/10.2205/2016ES000579

17. Gippius, F.N. and Myslenkov, S.A., 2020. Black Sea Wind Wave Climate with a Focus on Coastal Regions. *Ocean Engineering*, 218, 108199. https://doi.org/10.1016/j.oceaneng.2020.108199

18. Myslenkov, S., Zelenko, A., Resnyanskii, Y., Arkhipkin, V. and Silvestrova, K., 2021. Quality of the Wind Wave Forecast in the Black Sea Including Storm Wave Analysis. *Sustainability*, 13(23), 13099. https://doi.org/10.3390/su132313099

19. Booij, N., Ris, R.C. and Holthuijsen, L.H., 1999. A Third-Generation Wave Model for Coastal Regions. 1. Model Description and Validation. *Journal of Geophysical Research: Oceans*, 104(C4), pp. 7649-7666. https://doi.org/10.1029/98JC02622

20. Zijlema, M. and Van der Westhuysen, A.J., 2005. On Convergence Behaviour and Numerical Accuracy in Stationary SWAN Simulations of Nearshore Wind Wave Spectra. *Coastal Engineering*, 52(3), pp. 237-256. https://doi.org/10.1016/j.coastaleng.2004.12.006

21. Ratner, Yu.B., Fomin, V.V., Kholod, A.L. and Ivanchik, A.M., 2021. Updated System for the Sea Wave Operational Forecast of the Black Sea Marine Forecasting Center. *Physical Oceanography*, 28(5), pp. 579-595. https://doi.org/10.22449/1573-160X-2021-5-579-595

22. Fomin, V.V. and Polozok, A.A., 2021. Wind Waves in the Balaklava Bay under Extreme Wind Conditions. *Ecological Safety of Coastal and Shelf Zones of Sea*, (1), pp. 5-22. https://doi.org/10.22449/2413-5577-2021-1-5-22 (in Russian).

23. Zijlema, M., van Vledder, G.Ph. and Holthuijsen, L.H., 2012. Bottom Friction and Wind Drag for Wave Models. *Coastal Engineering*, 65, pp. 19-26. https://doi.org/10.1016/j.coastaleng.2012.03.002

24. Komen, G.J., Hasselmann, S. and Hasselmann, K., 1984. On the Existence of a Fully Developed Wind-Sea Spectrum. *Journal of Physical Oceanography*, 14(8), pp. 1271-1285. https://doi.org/10.1175/1520-0485(1984)014<1271:OTEOAF>2.0.CO;2

25. Madsen, O.S., Poon, Y.-K. and Graber, H.C., 1988. Spectral Wave Attenuation by Bottom Friction: Theory. *Coastal Engineering Proceedings*, 1(21), 34. https://doi.org/10.9753/icce.v21.34

26. Smolov, V.E. and Rozvadovskiy, A.F., 2020. Application of the Arduino Platform for Recording Wind Waves. *Physical Oceanography*, 27(4), pp. 430-441. https://doi.org/10.22449/1573-160X-2020-4-430-441

27. Yefimov, V.V., 1981. [*Dynamics of Wave Processes in the Boundary Layers of the Atmosphere and Ocean*]. Kiev: Naukova Dumka, 256 p. (in Russian).

28. Krogstad, H.E., 2005. Conventional Analysis of Wave Measurement Arrays. In: D. Hauser, K. Kahma, H.E. Krogstad, S. Lehner, J.A.J. Monbaliu and L.R. Wyatt, eds., 2005. *Measuring and Analysing the Directional Spectra of Ocean Waves*. Luxembourg: Office for Official Publications of the European Communities, pp. 56-71. https://doi.org/10.25607/OBP-811

29. Dulov, V., Kudryavtsev, V. and Skiba, E., 2020. On Fetch- and Duration-Limited Wind Wave Growth: Data and Parametric Model. *Ocean Modelling*, 153, 101676. https://doi.org/10.1016/j.ocemod.2020.101676

30. Yurovsky, Yu.Yu. and Dulov, V.A., 2020. MEMS-Based Wave Buoy: Towards Short Wind-Wave Sensing. *Ocean Engineering*, 217, 108043. https://doi.org/10.1016/j.oceaneng.2020.108043

31. Hauser, D., Tourain, C., Hermozo, L., Alraddawi, D., Aouf, L., Chapron, B., Dalphinet, A., Delaye, L., Dalila, M. [et al.], 2021. New Observations from the SWIM Radar On-Board CFOSAT: Instrument Validation and Ocean Wave Measurement Assessment. *IEEE Transactions on Geoscience and Remote Sensing*, 59(1), pp. 5-26. https://doi.org/10.1109/TGRS.2020.2994372

32. Hermozo, L., Rodriguez Suquet, R., Tourain, C., Hauser, D., Schippers, P., Aouf, L., Dalphinet, A., Sutherland, P., Marié, L., Gounou, A. [et al.], 2022. CFOSAT: Latest Improvements in the Swim Products and Contributions in Oceanography. In: GRSS, 2022. *IGARSS 2022 - 2022 IEEE International Geoscience and Remote Sensing Symposium*. IEEE, pp. 6768-6771. https://doi.org/10.1109/IGARSS46834.2022.9883958

33. Jiang, H., Mironov, A., Ren, L., Babanin, A.V., Wang, J. and Mu, L., 2022. Validation of Wave Spectral Partitions from SWIM Instrument On-Board CFOSAT against in Situ Data. *IEEE Transactions on Geoscience and Remote Sensing*, 60, 4204013. https://doi.org/10.1109/TGRS.2021.3110952

34. Mouche, A.A., Chapron, B., Zhang, B. and Husson, R., 2017. Combined Co- and Cross-Polarized SAR Measurements under Extreme Wind Conditions. *IEEE Transactions on Geoscience and Remote Sensing*, 55(12), pp. 6746-6755. https://doi.org/10.1109/TGRS.2017.2732508

35. Collard, F., Ardhuin, F. and Chapron, B., 2009. Monitoring and Analysis of Ocean Swell Fields from Space: New Methods for Routine Observations. *Journal of Geophysical Research: Oceans*, 114(C7), C07023. https://doi.org/10.1029/2008JC005215

36. Ovsienko, S.N., Fashchuck, D.J., Zatsepa, S.I., Ivchenko, A.A. and Petrenko, O.A., 2008. Storm of 11 November, 2007, in Srait of Kerch: Chronology of Events, Mathematical Modeling and Geographic/Ecological Analysis of Oil Spill. In: SOI, 2008. *Proceedings of SOI*. Moscow: SOI. Iss. 211, pp. 307-339 (in Russian).

37. Phillips, O.M., 1977. The *Dynamics of the Upper Ocean.* Cambridge, New York: Cambridge University Press, 336 p.

38. Hasselmann, K., Barnett, T.P., Bouws, E., Carlson, H., Cartwright, D.E., Enke, K., Ewing, J.A., Gienapp, H., Hasselmann, D.E. [et al.], 1973. Measurements of Wind-Wave Growth and Swell Decay during the Joint North Sea Wave Project (JONSWAP). *Ergänzungsheft zur Deutschen Hydrographischen Zeitschrift, Reihe A,* A8(12), pp. 1-95. https://doi.org/citeulike-article-id:2710264

39. Ardhuin, F., Chapron, B. and Collard, F., 2009. Observation of Swell Dissipation across Oceans. *Geophysical Research Letters*, 36(6), L06607. https://doi.org/10.1029/2008GL037030

40. Babanin, A.V. and Jiang, H., 2017. Ocean Swell: How Much Do We Know. In: ASME, 2017. *Proceedings of the ASME 2017 36th International Conference on Ocean, Offshore and Arctic Engineering.* Vol. 3A: Structures, Safety and Reliability, V03AT02A010. https://doi.org/10.1115/OMAE2017-61692

41. Babanin, A.V., Rogers, W.E., de Camargo, R., Doble, M., Durrant, T., Filchuk, K., Ewans, K., Hemer, M., Janssen, T. [et al.], 2019. Waves and Swells in High Wind and Extreme Fetches, Measurements in the Southern Ocean. *Frontiers in Marine Science*, 6, 361. https://doi.org/10.3389/fmars.2019.00361

42. Ardhuin, F., Rogers, E., Babanin, A.V., Filipot, J.-F., Magne, R., Roland, A., van der Westhuysen, A., Queffeulou, P., Lefevre, J.-M. [et al.], 2010. Semiempirical Dissipation Source Functions for Ocean Waves. Part I: Definition, Calibration, and Validation. *Journal of Physical Oceanography*, 40(9), pp. 1917-1941. https://doi.org/10.1175/2010JPO4324.1

43. Badulin, S.I. and Zakharov, V.E., 2017. Ocean Swell within the Kinetic Equation for Water Waves. *Nonlinear Processes in Geophysics*, 24(2), pp. 237-253. https://doi.org/10.5194/npg-24-237-2017

44. Kudryavtsev, V., Yurovskaya, M. and Chapron, B., 2021. 2D Parametric Model for Surface Wave Development under Varying Wind Field in Space and Time. *Journal of Geophysical Research: Oceans*, 126(4), e2020JC016915. https://doi.org/10.1029/2020JC016915

45. Yurovskaya, M., Kudryavtsev, V. and Chapron, B., 2023. A Self-Similar Description of the Wave Fields Generated by Tropical Cyclones. *Ocean Modelling*, 183, 102184. https://doi.org/10.1016/j.ocemod.2023.102184

46. Hay, A., Watson, C., Legresy, B., King, M. and Beardsley, J., 2023. In Situ Validation of Altimetry and CFOSAT SWIM Measurements in a High Wave Environment. *Journal of Atmospheric and Oceanic Technology*, 40(10), pp. 1137-1152. https://doi.org/10.1175/JTECH-D-23-0031.1

47. Woo, H.-J. and Park, K.-A., 2022. Validation of Significant Wave Height from Jason-3 and Sentinel-3A/B and Relation to Tidal Currents in Coastal Regions of the Korean Peninsula. *International Journal of Remote Sensing*, 43(3), pp. 961-996. https://doi.org/10.1080/01431161.2022.2026520

48. WAMDI Group, 1988. The WAM Model – A Third Generation Ocean Wave Prediction Model. *Journal of Physical Oceanography*, 18(12), pp. 1775-1810. https://doi.org/10.1175/1520-0485(1988)018<1775:TWMTGO>2.0.CO;2

49. Bertin, X., de Bakker, A., van Dongeren, A., Coco, G., André, G., Ardhuin, F., Bonneton, P., Bouchette, F., Castelle, B. [et al.], 2018. Infragravity Waves: From Driving Mechanisms to Impacts. *Earth-Science Reviews*, 177, pp. 774-799. https://doi.org/10.1016/j.earscirev.2018.01.002

50. Dolgikh, G.I. and Plotnikov, A.A., 2018. Peculiarities of Generation of Infragravity Waves. *Russian Meteorology and Hydrology*, 43(8), pp. 516-519. https://doi.org/10.3103/S1068373918080034

51. Nose, T., Babanin, A. and Ewans, K., 2024. Directional Characteristics of Infragravity Waves during Storms in the Nearshore Coastal Region. *Journal of Coastal Research*, 40(2), pp. 353-363. https://doi.org/10.2112/JCOASTRES-D-23-00015.1

Submitted 27.03.2024; approved after review 02.04.2024;
accepted for publication 11.04.2024.

About the authors:

Vladimir A. Dulov, Chief Researcher, Marine Hydrophysical Institute of RAS (2 Kapitanskaya Str., Sevastopol, 299011, Russian Federation), DSc (Phys.-Math.), **ORCID ID: 0000-0002-0038-7255**, **ResearcherID: F-8868-2014**, dulov1952@gmail.com

Maria V. Yurovskaya, Senior Researcher, Head of the Applied Marine Physics Laboratory, Marine Hydrophysical Institute of RAS (2 Kapitanskaya Str., Sevastopol, 299011, Russian Federation), CSc (Phys.-Math.), **ORCID ID: 0000-0001-6607-4641**, **ResearcherID: F-8957-2014**, mvkosnik@gmail.com

Vladimir V. Fomin, Chief Researcher, Marine Hydrophysical Institute of RAS (2 Kapitanskaya Str., Sevastopol, 299011, Russian Federation), DSc (Phys.-Math.), **ORCID ID: 0000-0002-9070-4460**, **ResearcherID: H-8185-2015**, v.fomin@mhi-ras.ru

Mikhail V. Shokurov, Leading Researcher, Marine Hydrophysical Institute of RAS (2 Kapitanskaya Str., Sevastopol, 299011, Russian Federation), DSc (Phys.-Math.), **ORCID ID: 0000-0003-1595-8281**, **ResearcherID: M-7160-2017**, shokurov.m@gmail.com

Yury Yu. Yurovsky, Leading Researcher, Head of the Applied Marine Physics Laboratory, Marine Hydrophysical Institute of RAS (2 Kapitanskaya Str., Sevastopol, 299011, Russian Federation), CSc (Phys.-Math.), **Scopus Author ID: 24377122700**, **ORCID ID: 0000-0002-9995-3965**, **ResearcherID: F-8907-2014**, y.yurovsky@mhi-ras.ru

Vladislav S. Barabanov, Senior Researcher, Head of the Applied Marine Physics Laboratory, Marine Hydrophysical Institute of RAS (2 Kapitanskaya Str., Sevastopol, 299011, Russian Federation), CSc (Phys.-Math.), **ORCID ID:0000-0002-2689-161X**, **ResearcherID: C-6007-2013**, wbarbs@gmail.com

Anton V. Garmashov, Senior Researcher, Head of the Applied Marine Physics Laboratory, Marine Hydrophysical Institute of RAS (2 Kapitanskaya Str., Sevastopol, 299011, Russian Federation), CSc (Geogr.), **ORCID ID: 0000-0003-4412-2483**, **ResearcherID: P-4155-2017**, ant.gar@mail.ru

Contribution of the co-authors:

Vladimir A. Dulov – general scientific supervision of the research; formulation of the goals and objectives; writing an article text; analysis of results and their interpretation; description and discussion of the research results; formulation of conclusions; critical text analysis

Maria V. Yurovskaya – collection of available materials on the research topic; analysis of results and their interpretation; data systematization, visualization and presentation; participation in the discussion of article materials and editing the article text; critical text analysis

Vladimir V. Fomin – participation in the discussion of article materials; software debugging; data processing; text editing

Mikhail V. Shokurov – participation in the discussion of article materials; text editing; software debugging; data processing

Yury Yu. Yurovsky – methodology, data processing; data visualization and presentation; participation in the discussion of article materials

Vladislav S. Barabanov – software debugging; data processing; participation in the discussion of article materials

Anton V. Garmashov – review of literature on the research problem; participation in the discussion of article materials and text editing

The authors have read and approved the final manuscript.
The authors declare that they have no conflict of interest.